

Biofabrication



PAPER


Tailoring nanostructure and bioactivity of 3D-printable hydrogels with self-assemble peptides amphiphile (PA) for promoting bile duct formation

RECEIVED
22 November 2017

REVISED
25 May 2018

ACCEPTED FOR PUBLICATION
31 May 2018

PUBLISHED
18 June 2018

M Yan¹ , P L Lewis^{1,2} and R N Shah^{1,2,3,4}

¹ Department of Biomedical Engineering Northwestern University, United States of America

² Simpson Querrey Institute, Northwestern University, United States of America

³ Department of Materials Science and Engineering, and Department of Surgery, Northwestern University, United States of America

⁴ Department of Surgery, Northwestern University, United States of America

E-mail: ramille-shah@northwestern.edu

Keywords: 3D bioprint, bioink, peptides amphiphilie, IKVAV, cholangiocyte

Supplementary material for this article is available [online](#)

Abstract

3D-printing has expanded our ability to produce reproducible and more complex scaffold architectures for tissue engineering applications. In order to enhance the biological response within these 3D-printed scaffolds incorporating nanostructural features and/or specific biological signaling may be an effective means to optimize tissue regeneration. Peptides amphiphiles (PAs) are a versatile supramolecular biomaterial with tailorable nanostructural and biochemical features. PAs are widely used in tissue engineering applications such as angiogenesis, neurogenesis, and bone regeneration. Thus, the addition of PAs is a potential solution that can greatly expand the utility of 3D bioprinting hydrogels in the field of regenerative medicine. In this paper, we firstly developed a 3D-printable thiolated-gelatin bioink supplemented with PAs to tailor the bioactivity and nanostructure which allows for the incorporation of cells. The bioink can be printed at 4 °C and stabilized to last a long time (>1 month) in culture at 37 °C by via a dual secondary crosslinking strategy using calcium ions and homobifunctional maleimide-poly (ethylene glycol). Rheological properties of inks were characterized and were suitable for printing multi-layered structures. We additionally demonstrated enhanced functionality of ink formulations by utilizing a laminin-mimetic IKVAV-based PA system within a 3D-printable ink containing cholangiocytes. Viability and functional staining showed that the IKVAV PA nanofibers stimulated cholangiocytes to form functional tubular structures, which was not observed in other ink formulations.

1. Introduction

Three-dimensional (3D) scaffolds fabricated by 3D bioprinting show significant promise in tissue engineering and regenerative medicine applications in addition to *in vitro* platforms for disease models and high throughput drug screening and testing [1, 2]. In the field of 3D bioprinting, bioinks are synthetic or natural biomaterials which are printable with or without cells and signal molecules such as growth factors and cytokines to mimic the environment of target tissues [3–6]. One of the challenges is to develop suitable materials for use as tunable bioinks to meet the requirements for various biomedical applications while maintaining printability [7].

To meet the printability and mechanical properties requirements for bioprinting, many materials (alginate, gelatin, fibrin, collagen, chitosan, HA) [8–14] can be used with most gel printing strategies involving an initial (primary) crosslinking step and a secondary crosslinking step, such as adding in calcium in alginate systems [15], or UV crosslinking PEGDA [16]. Gelatin, for example, is biocompatible and shows concentration- and temperature-dependent gelation properties. Lightly crosslinked gelatin suitable for printing, however, cannot support itself in long term culture conditions. Rutz *et al* utilized a two-step crosslinking method to print lightly crosslinked materials followed by secondary crosslinking to strengthen the material [3], which was successful in prolonging the

long term culture of the printed cell-laden hydrogel scaffolds.

For cells to survive and perform a desired function, the bioink must also provide necessary signaling molecules such as cell adhesion motifs or functional peptides [17]. In recent years, researchers have developed many advanced strategies for fabricating biomimetic nanofibrous scaffolds designed to mimic the extracellular matrix (ECM) [18, 19]. Peptide amphiphiles (PAs) are a class of self-assembling molecules that can assemble into nanofibers [20]. Peptide amphiphiles (PAs) are a class of self-assembling molecules that can assemble into nanofibers [21, 22]. Various PAs have been developed and modified for different applications in tissue engineering and regenerative medicine including ischemic tissue repair [23], neurogenesis [24, 25], and bone regeneration [26]. With a better understanding of how cells interact with the extracellular matrix, more specific PAs can be designed to enhance the functionality of tissue engineering systems. However, as an injectable material whose gelation depends on ions like calcium, the weak mechanical properties limit the applications of PA nanofibers alone for organ and sub-organ scale tissue engineering and regenerative medicine. Rutz *et al* demonstrated the successful incorporation of PAs (containing no bioactive epitope) into bioinks to add robustness and nanostructure to the printed structures, however, the biological effect of PA incorporation within the bioinks was not assessed [3]. The work presented here is the first to assess the cellular response of printed structures containing bioactive PAs. Creating a 3D-printable bioink containing PA nanofibers may be a way to leverage the bioactivity, multifunctional potential, and biomimetic nanostructure of PAs while being able to form self-supporting and complex scaffolds necessary for multi-tissue and organ engineering.

In this work we used thiolated-gelatin as a matrix to incorporate PA nanofibers and facilitate 3D-printing while preserving the nanostructure. For an application, we tested the bioactivity of a laminin-derived peptide sequence IKVAV (Ile-Lys-Val-Ala-Val) within the bioinks and investigated its influence on biliary epithelial cells (cholangiocytes). Laminin is an extracellular matrix molecule found in the basement membrane, is necessary for cell adhesion and polarization, and is widely used in neuroengineering [24]. There are reports that laminin can promote polarization of cholangiocytes to form bile ducts [27]. There are, however, no investigations into the interactions between IKVAV PAs and cholangiocytes. To the best of our knowledge, this is the first-time peptide amphiphiles have been integrated within a 3D-printable system for a specific biological application-intrahepatic bile duct tissue engineering. We mixed thiolated-gelatin, different mixtures of PAs, and cholangiocytes at 37 °C and 3D-printed the scaffold at 4 °C. The gelatin formed a

physical gel due to the thermal difference which is reversible. 3D-printed scaffolds were stabilized for long term culture with the addition of a secondary crosslinking solution containing calcium ions and homobifunctional maleimide-conjugated polyethylene glycol (PEG-MAL) to maintain PA nanofibers and cross-link the thiolated-gelatin. Bioink physical characteristics were measured using a rheometer and SEM imaging, while encapsulated cell experiments evaluated bioactivity.

2. Materials and method

2.1. Material preparation

2.1.1. Thiolated-gelatin synthesis

Thiolated-gelatin was synthesized as previously described in [28]. Briefly, 1 g gelatin was dissolved in 72.5 ml reaction buffer (93.2 mM Na₂HPO₄, 6.8 mM NaH₂PO₄, 0.584 mg ml⁻¹ EDTA, pH 8) at 37 °C for 60 min. Then 27.5 ml of a 0.2 wt% Traut's reagent (2-iminothiolane hydrochloride, Sigma) solution, dissolved in reaction buffer, was added at 40 °C for 2 h. To break any disulfide bonds, 573.3 mg TCEP (tris(2-carboxyethyl) phosphine hydrochloride, Sigma) was added to the reaction mixture for 15 min, followed by lowering the pH to 2. Thiolated-gelatin (Gel-SH) was dialyzed against pH 2 purified water with 12 k MWCO dialysis tubing for 3 h at 40 °C followed by 5 days at 4 °C to remove residual Traut's reagent and TCEP. Gel-SH was then sterile filtered with 0.22 μm PVDF filters and lyophilized for 72 h. Gel-SH foam was stored at -80 °C until use.

2.1.2. Peptides amphiphile (PA)

PAs were synthesized as previously described [29] using standard solid phase synthesis. Two PA sequences used were CH₃(CH₂)₁₅VVAAEEIKVAV (IKVAV) and CH₃(CH₂)₁₅VVAAEE (E2). Lyophilized PAs were dissolved in 150 mM NaCl and 3 mM KCl and gelled with the addition of 25 mM CaCl₂. E2 was dissolved to make a 2 wt% solution at pH 7.4. IKVAV solutions consisted of mixtures of 80 mol% E2 and 20 mol% IKVAV PAs at a total of 2 wt% with 7.4 pH. Both E2 and IKVAV solutions were bath sonicated for 15 min and incubated at 60 °C for 30 min, then cooled to room temperature [30].

2.2. Bioink preparation

We investigated a series of formulations of bioinks shown in (table 1). For the gelatin-only group, the Gel-SH solution was diluted with culture medium (with or without cells) to 3 wt%. For IKVAV-ink and E2-ink, Gel-SH ratios were combined at a 3:1 ratio, the final components being 2.25 wt% Gel-SH, 0.75 wt% mixture PA (80 mol% E2, 20 mol% IKVAV) or 0.75 wt% E2, dissolved in culture medium with or without cells. Aseptic technique was employed with all materials involved in cell culture. Gel-SH solutions, or Gel-SH/PA solutions were gelled using a secondary

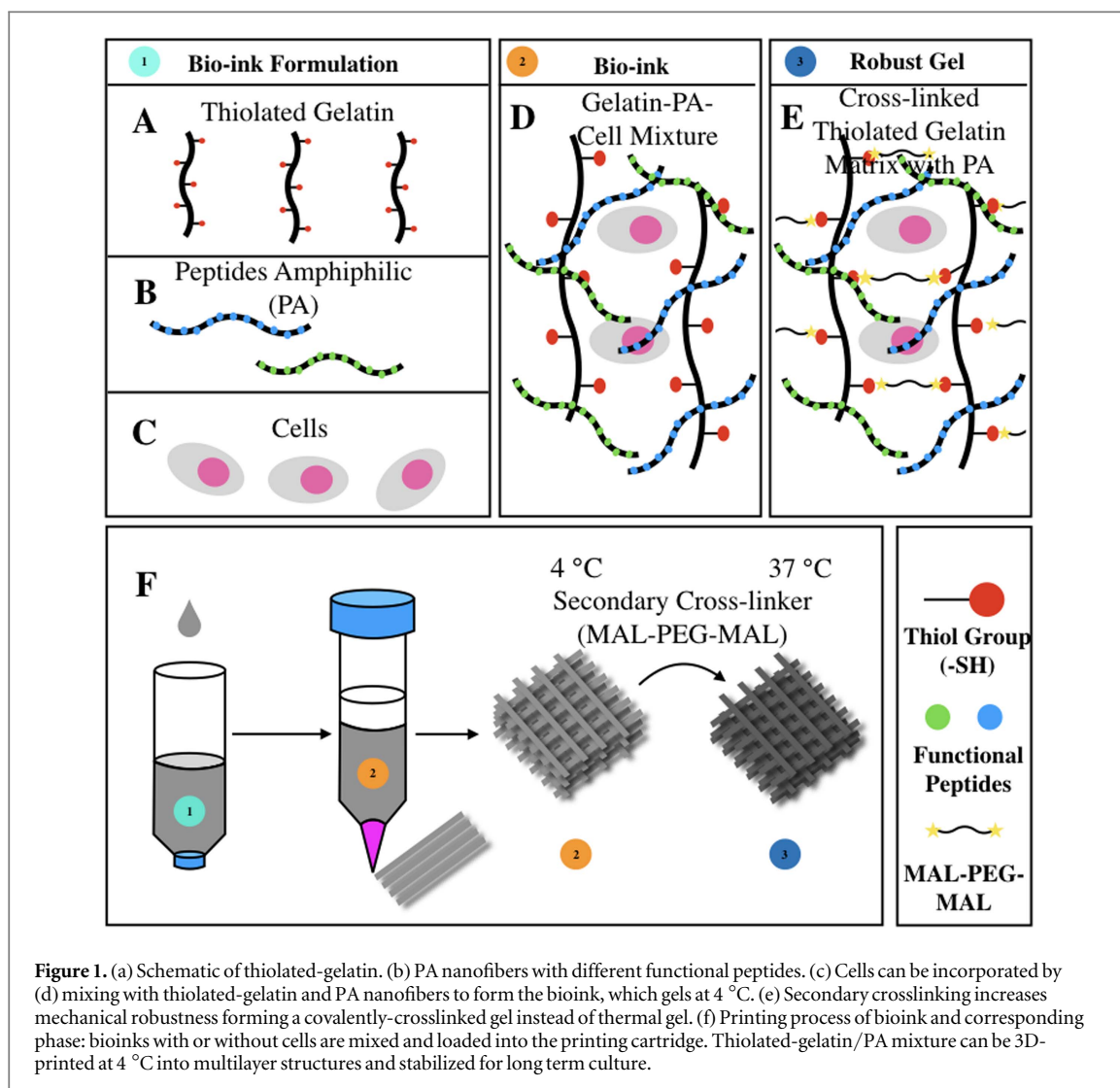


Table 1. Formulas of bioinks.

Bioink	Thiolated-gelatin	PA	Cells
Gelatin-ink	3 wt%	0	with/without
E2-ink	2.25 wt%	0.75 wt% E2 PA	with/without
IKVAV-ink	2.25 wt%	0.75 wt% mixture PA (80 mol% E2 PA and 20 mol% IKVAV PA)	with/without

crosslinking solution of 25 mM CaCl_2 supplemented with 5% 5 K MW homobifunctional maleimide-poly (ethylene glycol)-maleimide (MAL-PEG-MAL, Laysan Bio).

2.3. Rheological characterization

Testing was performed using an Anton-Paar MCR 302 rheometer with a parallel-plate geometry (PP25/TG parallel-plate 24.982 mm diameter and 0.5 mm gap). The temperature was controlled at 37 °C at the beginning of testing and rapidly cooled to 4 °C. Formulations of bioinks were prepared at 37 °C and

loaded on the warmed plate and the measuring cone was lowered into position. Mineral oil was then applied to the edges to prevent dehydration. An oscillatory time sweep was performed for 3000 s and followed by a frequency sweep from 0.1 to 100 rad s^{-1} which 31 points were collected and then amplitude sweep was performed from 0.01% to 1.00E4% shear strain and 61 points was collected by the rheometer automatically with 10 dec^{-1} . Temperature was controlled at 37 °C during testing. After a 3000 s time sweep test, a frequency sweep and then an amplitude sweep were performed using testing parameters described above. In order to assess the efficacy of using the secondary crosslinker to stabilize the hydrogel, after a time sweep, the secondary crosslinker solution was added to the bioink and the plate was warmed rapidly to 37 °C.

2.4. Bioprinting

Sterile bioinks with or without cells were prepared in the cell culture hood at 37 °C and transferred to 30cc Nordson EFD cartridges. The cartridges were stored

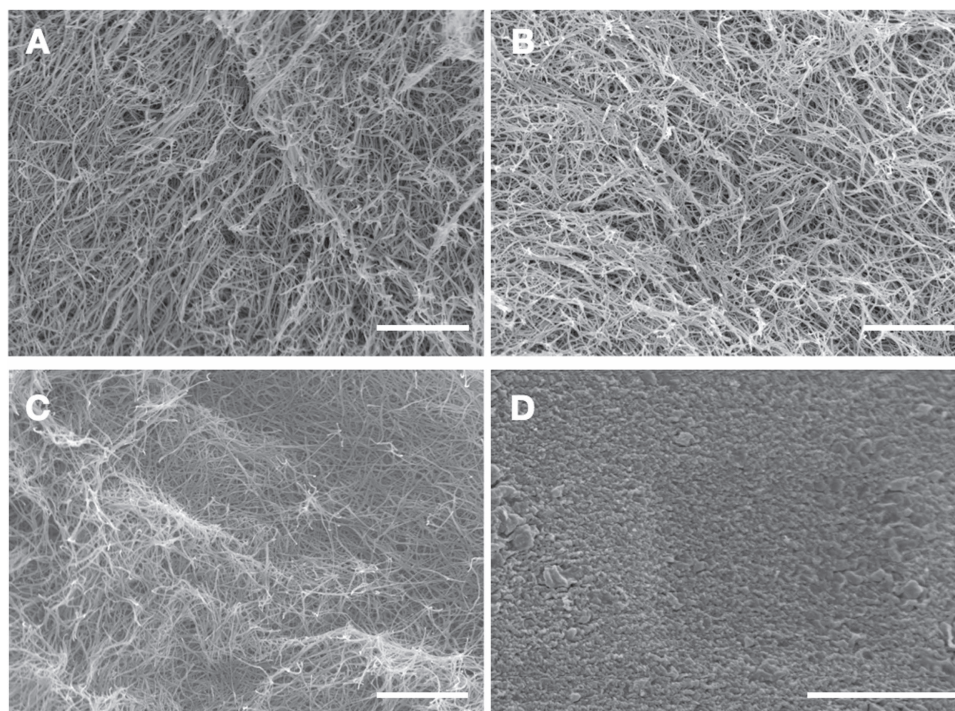


Figure 2. SEM images of different mass ratios of thiolated-gelatin: PA. (a) 1:3 mass ratio. (b) 1:1 mass ratio. (c) 3:1 mass ratio. (d) 1:0 mass ratio (pure thiolated-gelatin). All the scale bars are 2 μm .

within the printing magazine to equilibrate to 4 °C for 20 min. Bioinks were 3D-printed with an Envision TEC (GMBH) 3D-Bioplotter onto sterile autoclaved glass slides at 4 °C with a nozzle diameter of 250 μm . Printing pressure was 0.6 bar and print speed was 10 mm s⁻¹. After printing, the scaffolds were soaked in the secondary crosslinking solution and incubated at 37 °C for 15 min. The scaffolds with cells were washed with PBS and incubated in culture medium. Scaffolds were imaged for viability and morphology at 4, 7, 14, and 21 day time points.

2.5. Cell culture

Cells used in these experiments were SV40 immortalized mouse cholangiocytes (SV40SM), a gift from the laboratory of Professor Gianfranco Alpini [31, 32]. Growth medium consists of modified Eagle medium (MEM) supplemented with 10% FBS (Gibco), L-glutamine, and penicillin/streptomycin (Gibco). After 24 h of gel culture, medium was changed to Williams medium E supplemented with insulin (100 nmol l⁻¹), hydrocortisone (5 mol l⁻¹), and penicillin/streptomycin [31, 32].

2.6. Viability imaging

The samples were washed with warm PBS twice and stained with Live/Dead (calcein AM/ethidium homodimer) viability stain (Molecular Probes). After 30 min incubation, the stain solution was removed and samples were imaged with a Nikon C2+ laser scanning confocal microscope.

2.7. Cholyl-lysyl-fluorescein (CLF) imaging

Negative control groups were incubated in culture media supplemented with 100 μM Rifampicin (Sigma) for 24 h. Cultures were washed with Hank's balanced salt solution (HBSS) and incubated in 5 μM CLF (Corning) for 60 min. Samples were then washed and incubated for an additional 45 min in culture medium. The samples were then imaged with a Nikon C2+ laser scanning confocal.

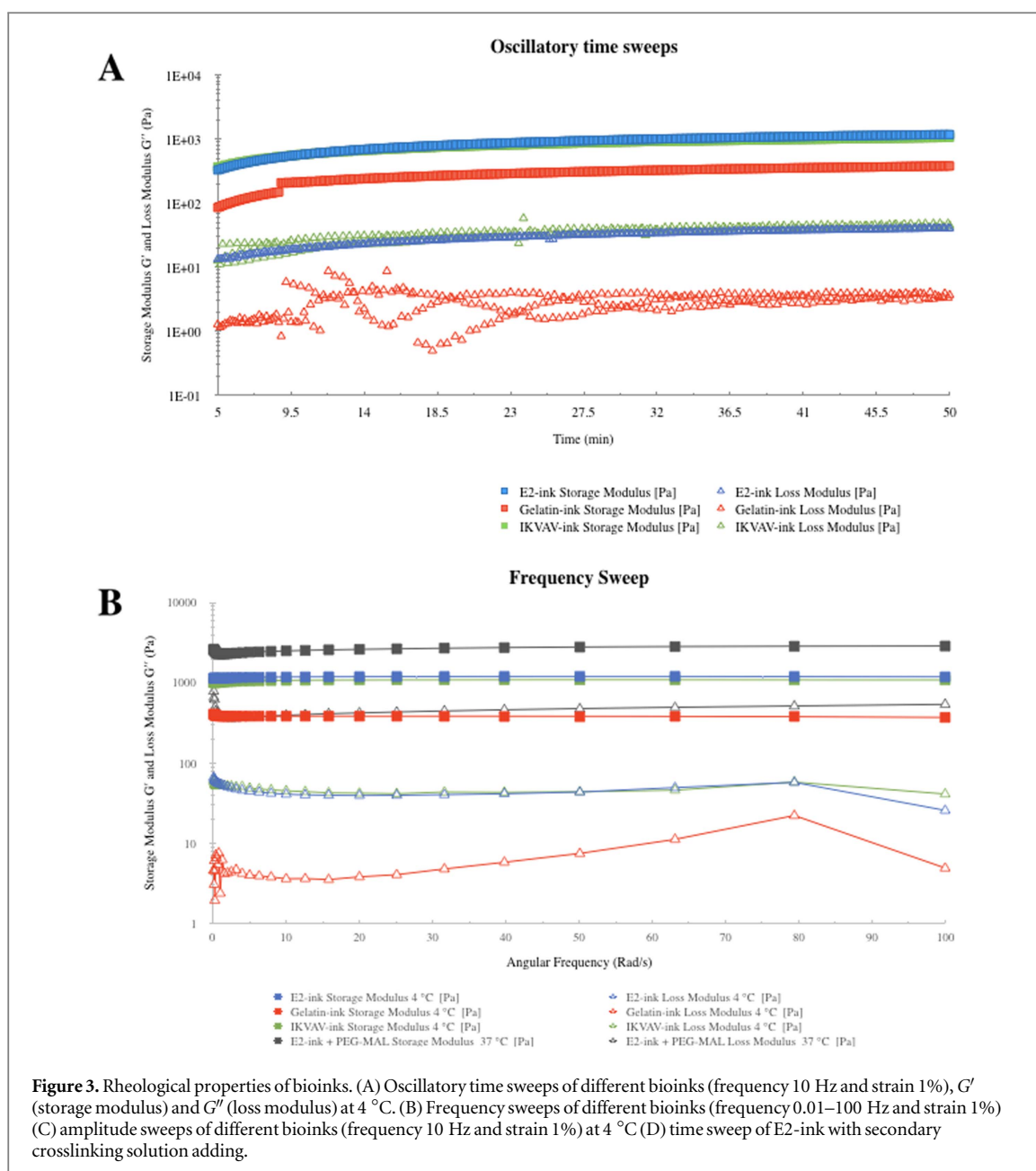
2.8. SEM analysis

The samples were fixed by 3 wt% glutaraldehyde-2% sucrose solution and subsequently dehydrated using an ethanol series. Samples were critical point dried using Autosamdri-795 and osmium coated using SPF Osmium coater. SEM analysis was performed with a LEO Gemini 1525.

3. Results and discussion

3.1. The preparation of bioinks

Previous work in our lab has explored a series of gelatin-based bioinks which show that the 3 wt% total polymer is suitable for 3D-printing [3]. Low concentrations of gelatin are easy to manipulate for printing and facilitate nutrient diffusion. Thus, we kept the 3 wt% in all bioinks tested. The thiolated-gelatin shares the same properties as the normal gelatin: it forms reversible physical gel at low temperatures (4 °C) and liquefies at higher temperatures (37 °C). Meanwhile, thiolated-gelatin can be crosslinked by



homobifunctional maleimide-conjugated polyethylene glycol (MAL-PEG-MAL) in less than one minute at 37 °C to form a robust gel [33]. PAs will self-assemble into supramolecular nanofibers when the PA solution was cooled from 65 °C to 25 °C at pH 7–8 for several hours [30]. Preliminary experiments showed that the annealing process enhances printability and increasing the robustness of the resulting scaffold. Thiolated-gelatin was mixed with pre-annealed PA at 37 °C with or without cells (figures 1(a)–(d)) and chilled to 4 °C. The thiolated-gelatin was 3D-printed (figure 1(f)) onto a 4 °C substrate and treated with a secondary crosslinking solution to stabilize the gel (figures 1(e) and (f)) at 37 °C.

To demonstrate how mass ratio of thiolated-gelatin to PA influences nanofiber formation, 4 groups of

secondary-crosslinked bioinks with mass ratios of thiolated-gelatin: PA (3:1, 1:1, 1:3, 1:0) were visualized under SEM (figure 2). In mass ratios thiolated-gelatin: PA (1:3, 1:1, 3:1) (figures 2(a)–(c)) the nanofibers can be observed while there was no fiber structure in the pure thiolated-gelatin sample. The density of nanofibers increased with the increasing of the mass proportion of PA, however the printability decreased. These results indicated we successfully mixed PAs with thiolated-gelatin to create a printable formulation that incorporates a nanofibrous network compared to pure thiolated-gelatin. These fibers add nanostructural features and provide tailorable bioactivity that is necessary for cell-matrix interactions that promote cell adhesion and influence cell function. We opted to proceed with a thiolated-gelatin: PA mass ratio of (3:1) for the

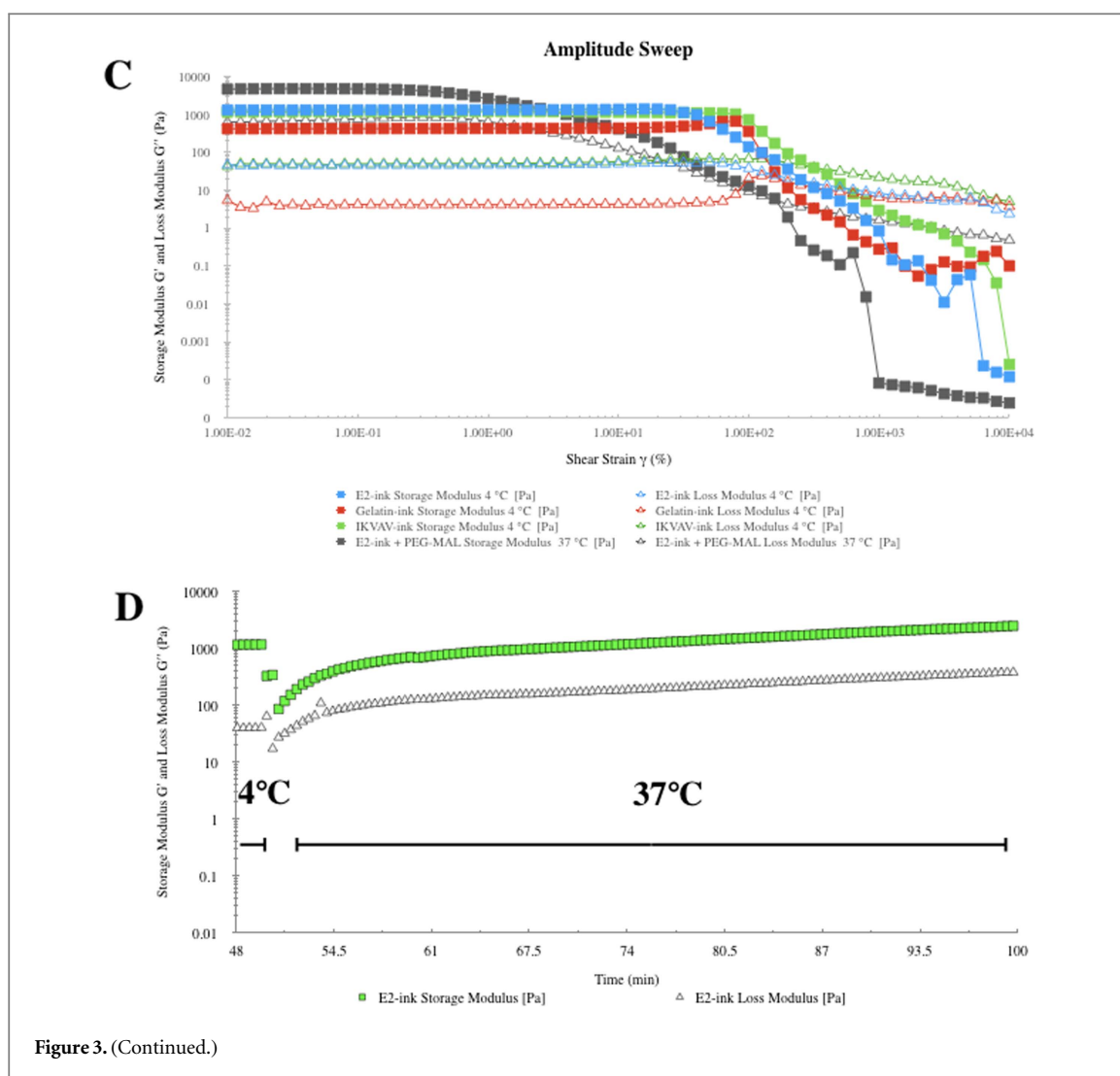


Figure 3. (Continued.)

remainder of our experiments, as it shows the best compromise between printability and nanofiber formation.

3.2. Rheological properties

A series of rheological tests were carried out to investigate the rheological properties of the bioinks investigated. The oscillatory time sweeps of E2-ink, Gelatin-ink and IKVAV-ink (1% strain, 10 rad s⁻¹ angular frequency) were performed for 3000 s at 4 °C (figure 3(a)). In all the three bioinks, storage modulus (G') was much higher than the loss modulus (G'') ($G' \gg G''$) indicating bioinks display the behavior of a viscoelastic solid. Storage moduli were mostly stable by 14 min, but displayed modest growth over longer times. The bioinks therefore stabilize fast enough to prevent cell stress due to prolonged time at low temperatures. The complex shear modulus (G^*) describes the entire viscoelastic of a sample and can be calculated by the formula (1).

$$G^{*2} = G'^2 + G''^2. \quad (1)$$

Comparing the complex shear moduli (G^*) (supplementary table 1 is available online at stacks.iop.org/BF/10/035010/mmedia), higher complex shear

modulus (G^*) is observed in the E2-ink (~1130 Pa) and IKVAV-ink (~1022 Pa) compared to the thiolated-gelatin-ink alone (~365 Pa). This can be due to the PA nanofibers enhancing the robustness of the bioinks. Of note is that comparing with Gelatin-ink in mechanical properties is similar in both the E2 PA and IKVAV PA formulations are stronger in mechanical properties. Frequency sweep tests of E2-ink, thiolated-gelatin-ink, and IKVAV-ink (1% strain) were performed at 4 °C following the time sweep. In all the three bioinks, storage modulus (G') were observed to be much higher than the loss modulus (G'') ($G' \gg G''$) and no crossover point was found in any bioink. The results indicate that all the bioinks are stable over the duration of printing.

The amplitude sweeps of E2-ink, Gelatin-ink and IKVAV-ink (10 rad s⁻¹ angular frequency) were performed at 4 °C after the frequency sweeps. Amplitude sweeps describe the deformation behavior of bioinks which influences hydrogel extrusion and the structural integrity of the filaments during printing. In all bioinks, G'' surpassed G' beyond the linear viscoelastic region (LVE region) at high strains (figure 3(c)), indicative of shear-thinning. Shear-thinning behavior

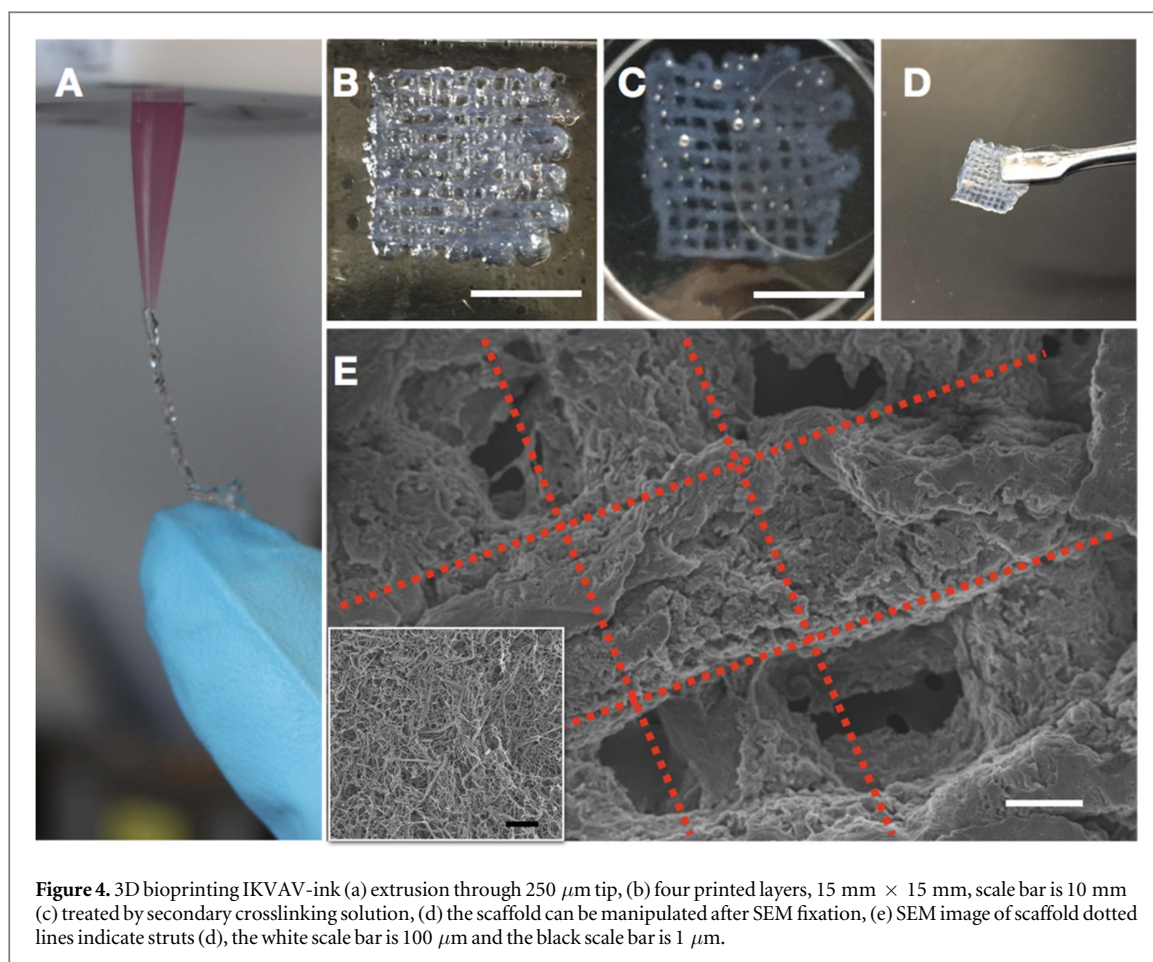


Figure 4. 3D bioprinting IKVAV-ink (a) extrusion through 250 μm tip, (b) four printed layers, 15 mm \times 15 mm, scale bar is 10 mm (c) treated by secondary crosslinking solution, (d) the scaffold can be manipulated after SEM fixation, (e) SEM image of scaffold dotted lines indicate struts (d), the white scale bar is 100 μm and the black scale bar is 1 μm .

describes the bioink behavior at high shear environments and is necessary for successful printing. An increase in liquid-like properties is beneficial for hydrogel extrusion as it reduces the pressure needed for printing, and it is also gentler on encapsulated cells. It was also observed that the strain at which G'' exceeded G' increased when the PA nanofibers are present (the crossover of Gelatin-ink, E2-ink, and IKVAV-ink were around 220%, 280%, 310% strain, respectively). For this system, secondary cross linkers are necessary after printing as scaffolds will degrade at 37 $^{\circ}\text{C}$ in culture medium. We opted to take advantage of both PA and thiolated-gelatin gelation mechanisms using calcium ions and PEG-MAL, respectively. Rheological results showed that the secondary crosslinker was effective at stabilizing the gel at 37 $^{\circ}\text{C}$ as shown in figure 3(d).

3.3. 3D-printing of bioinks

To test the printability, we printed IKVAV-ink encapsulating biliary epithelial cells (cholangiocytes) (0.2×10^6 cells ml^{-1}) (video 5). The results (figure 4(a)) show that IKVAV-ink can be extruded through a 250 μm diameter nozzle with 0.9 bar pressure in a self-supporting multi-layered structure that maintained structural integrity (sup video 1). A layer-by-layer self-supporting scaffold can be 3D-printed (figure 4(a)) in a variety of other geometries (figures S1

and S2). Figures 4(c)–(e) and S2 show the scaffold treated with the secondary crosslinker prevented the structure from collapsing when picked up with forceps. The rapid thiol-maleimide reaction prevented scaffold dissolution in addition to structural collapse.

3.4. Cell experiments

Cholangiocytes were mixed within the inks at 200 000 cells ml^{-1} and 200 μl bioinks were extruded through a 250 μm diameter nozzle with 0.6 bar pressure into confocal petri dishes. After that, the cells were cultured for 4, 7, and 14 days. After 4 days of culture, cholangiocytes formed round cysts with luminal space in the Gelatin-ink and IKVAV-ink (figures 5(a) and (m)). When the cysts were kept in culture for three days, the cysts in the Gelatin-ink were still round and became larger (figure 5(b)) while the cysts in IKVAV-ink were able to bud and formed branching tubular structures (figure 5(n)). After one more week in culture, the cysts in the Gelatin-ink continued to grow but did not have morphological changes (figure 5(c) and video 1). Meanwhile, more buds were observed in the IKVAV-ink (figure 5(o) and video 3). During the 14 days in culture, cholangiocytes in the E2-ink did not form cysts or buds, they formed clusters which were not round but had no tendency to form buds or tubular structures (figures 5(g)–(i) and video 2). Depth-coded images suggest the

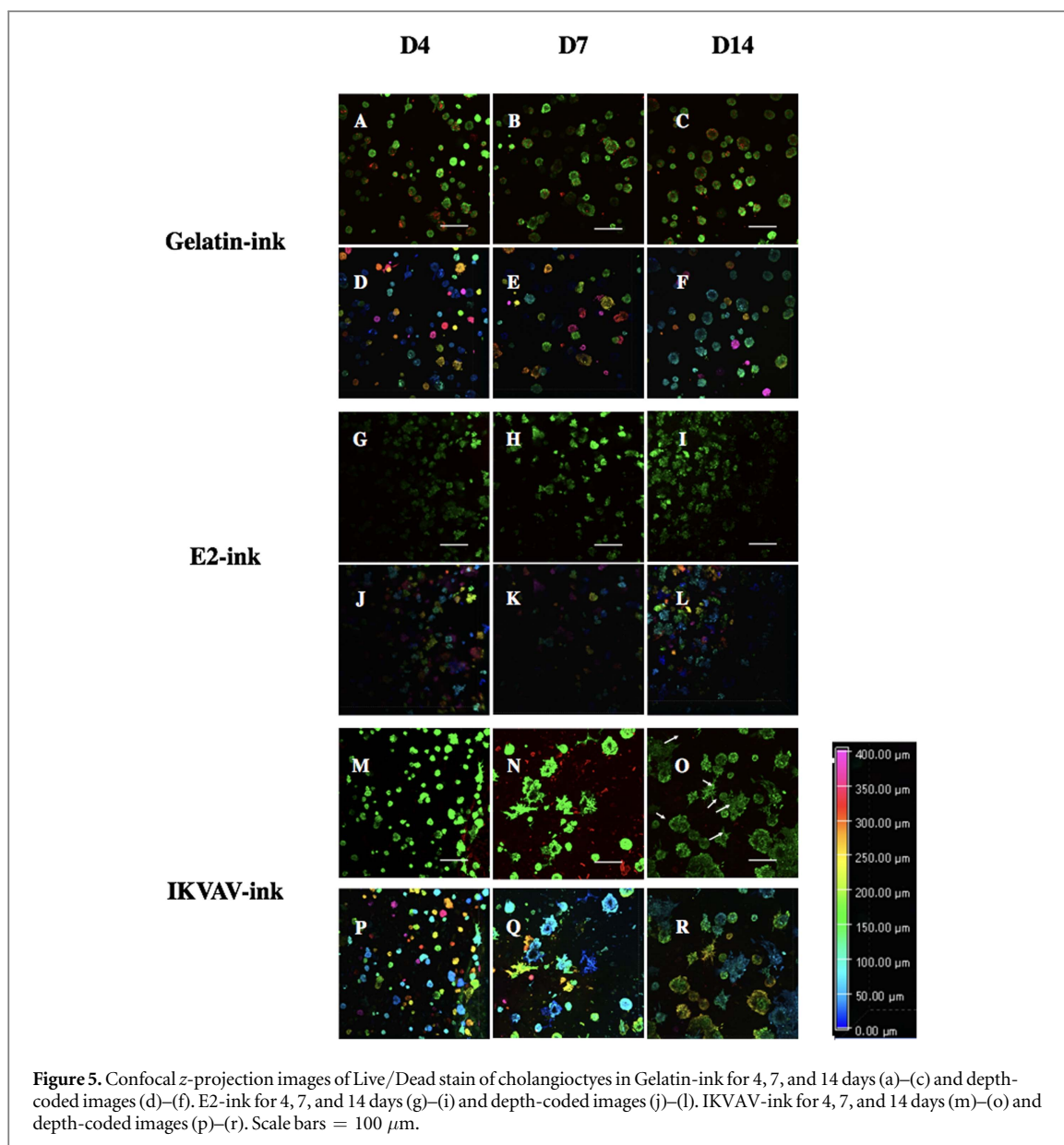


Figure 5. Confocal z-projection images of Live/Dead stain of cholangiocytes in Gelatin-ink for 4, 7, and 14 days (a)–(c) and depth-coded images (d)–(f). E2-ink for 4, 7, and 14 days (g)–(i) and depth-coded images (j)–(l). IKVAV-ink for 4, 7, and 14 days (m)–(o) and depth-coded images (p)–(r). Scale bars = 100 μm .

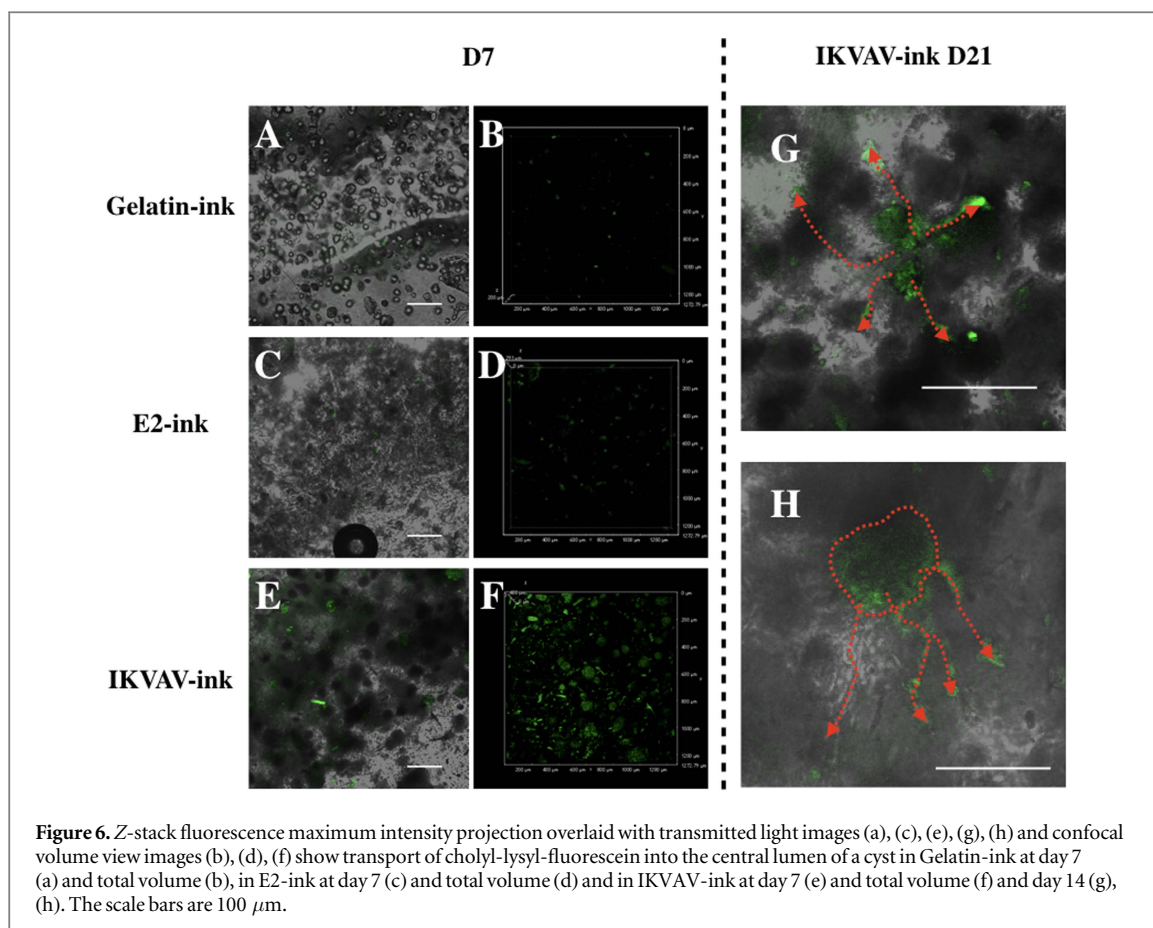
cells were located at different depths within the gels (figures 5(d)–(f), (j)–(l) and (p)–(r)).

The E2 PA does not contain any functional peptides and works as a filler to the other functional PAs within the fiber structure [24]. Comparing cells in E2-ink and the IKVAV-ink, the IKVAV peptides seemed to successfully stimulate the formation of tubular structure.

One of the main functions of mature cholangiocytes is the ability to transport cholesteryl-lysyl-fluorescein (CLF, a fluorescein-labeled bile acid analog that closely parallels the cellular binding and uptake properties of cholic acid derivatives) into the central lumen [34]. When cysts were incubated with cholesteryl-lysyl-fluorescein (CLF), fluorescence accumulation was detected inside the cells and central lumen. In the samples of E2-ink and Gelatin-ink, a small quantity of cysts was able to transport the CLF (figures 6(a)–(d)) while more functional cysts and a larger volume of CLF accumulation is observed in the IKVAV-ink (figures 6(e) and

(f)). Furthermore, after an additional week in culture, the CLF accumulation in the lumen of the IKVAV-ink sample showed tubular structures extending from the central cyst structures (figures (g), (h) and video 4).

During the cholangiopathies such as primary sclerosing cholangitis (PSC), cholangiocarcinoma and cystic fibrosis (CF), ductular reaction is apparently an attempt to activate endogenous repair mechanisms but can also be viewed as an abnormal regenerative response because it is accompanied by excessive extracellular matrix deposition and promotes the progression of fibrosis [35, 36]. ‘Ductular reactive cells’ (DRCs), are immature cholangiocytes (small cholangiocytes) that coalesce into primitive, but with non-functional, duct-like structures. DRCs, however, have the potential to differentiate into mature (large) cholangiocytes and form functional bile ducts [37]. We hypothesize that a similar phenomenon is occurring in these artificial gel environments where in certain situations, the small cholangiocytes form cysts



and are not functional and in other scenarios where the right signaling is provided the small cholangiocytes differentiate into a more mature phenotype that results in the start of duct formation with added function.

The increase in function occurred most significantly with the incorporation of the IKVAV PA within the bioink. Laminin plays an important role in bile ducts formation [27], where targeting studies have shown that cholangiocyte specification is mediated by the interaction of the Notch signaling pathway [38]. Not only does Notch signaling play a critical role in intrahepatic bile duct morphogenesis in mice, but it is also involved in cholangiocyte development in humans [39–43]. The Ile-Lys-Val-Ala-Val (IKVAV) sequence is derived from laminin-1 which has been used as neuron cell adhesion and polarization peptides for decades [44]. To our knowledge, this work is the first to explore the use of a self-assembling IKVAV-containing peptide amphiphile to induce small cholangiocyte maturation and enhance function. According to our results, incorporation of the IKVAV peptide amphiphile in the bioink was able to more effectively lead to cholangiocyte maturation and the start of functional duct formation, which we hypothesize to be induced through the Notch 2 signaling pathway. Although more experiments are needed to further understand the mechanism behind it, these initial studies using PA-containing bioinks are promising and

presents a potential new treatment for cholangiopathies where induction of immature cholangiocytes into mature cholangiocytes is the main goal.

The 3D-printing of gelatin inks containing IKVAV PA has the potential to promote and control intrahepatic bile duct formation. Because of the wide variety of bioactive PA sequences available, 3D-printing with PAs has numerous potential applications in tissue engineering, especially in the field of complex functional tissue regeneration. For instance, fabricating functional liver tissue *in vitro* containing blood vessels, intrahepatic bile ducts and hepatocytes would require the use of complex CAD models to spatially pattern different PA-containing bioinks and cell types to build fully functional tissue. More work will need to be done to study the interaction of different cells before achieving this goal, however, but 3D-printing PA-containing bioinks has enormous potential in the tissue engineering field.

4. Conclusion

PA nanofibers can be mixed into thiolated-gelatin bioinks, successfully 3D-printed, and contribute nanostructural features and bioactivity to the printed structures. The presence and concentration of PAs within the bioinks influence the rheological properties of the bioinks as well as the density of nanofibers present in the resulting printed structures. At 4 $^{\circ}\text{C}$, the

bioinks can be printed into filaments which retain integrity during printing and have the ability to support multi-layered scaffolds. The scaffolds were successfully strengthened using a secondary cross-linking solution, which also stabilized the scaffolds for long term culture. *In vitro* experiments demonstrated high cell viability after printing and throughout the culture period. Cholangiocytes showed enhanced morphological changes (i.e. formation of functional tube structures and rudimentary bile ducts) when cultured in the IKVAV-ink compared to the gelatin-ink and E2-ink. Future optimization of peptide concentration and incorporating other signaling moieties within the bioinks are necessary to further enhance the formation of functional duct and branching structures reminiscent of what is seen in the natural liver structure. These results, however, demonstrate the promise of using this bioink system to successfully integrate self-assembling PAs within 3D-printed structures to incorporate nanostructural features as well as targeted and multifunctional bioactivity that can be utilized for a variety of complex tissue engineering applications. In addition to bioprinting, the PA bioinks can also provide versatile *in vitro* culture systems for disease modeling (e.g. primary sclerosing cholangitis or cholangiocarcinoma) and drug discovery/screening applications.

Acknowledgments

Imaging work was performed at the Northwestern University Center for Advanced Microscopy generously supported by NCI CCSG P30 CA060553 awarded to the Robert H Lurie Comprehensive Cancer Center. Rheometry using the Anton-Paar MCR 302 rheometer was performed in the Analytical BioNano-Technology Core Facility of the Simpson Querrey Institute (SQI) at Northwestern University. The US Army Research Office, the US Army Medical Research and Materiel Command, and Northwestern University provided funding to develop SQI and ongoing support is being received from the Soft and Hybrid Nanotechnology Experimental (SHyNE) Resource (NSF NNCI-1542205). This work was supported by the National Institutes of Health grant number 1K01DK099454. The authors thank Professor Gianfranco Alpini for providing Cholangiocytes.

ORCID iDs

M Yan  <https://orcid.org/0000-0002-4561-9187>

References

- [1] Derby B 2012 Printing and prototyping of tissues and scaffolds *Science* **338** 921–6
- [2] Mironov V, Kasyanov V and Markwald R 2011 Organ printing: from bioprinter to organ biofabrication line *Curr. Opin. Biotechnol.* **22** 667–73
- [3] Rutz A, Hyland K, Jakus A, Burghardt W and Shah R 2015 A multimaterial bioink method for 3D printing tunable, cell-compatible hydrogels *Adv. Mater.* **27** 1607–14
- [4] Gao B, Yang Q, Zhao X, Jin G, Ma Y and Xu F 2016 4D bioprinting for biomedical applications *Trends Biotechnol.* **34** 746–56
- [5] Yang Q, Lian Q and Xu F 2017 Perspective: fabrication of integrated organ-on-a-chip via bioprinting *Biomicrofluidics* **11** 031301
- [6] Ma Y *et al* 2017 Bioprinting-based PDLSC-ECM screening for *in vivo* repair of alveolar bone defect using cell-laden, injectable and photocrosslinkable hydrogels *ACS Biomater. Sci. Eng.* **3** 3534–45
- [7] Jakus A, Rutz A and Shah R 2016 Advancing the field of 3D biomaterial printing *Biomed. Mater.* **11** 014102
- [8] Yan Y *et al* 2005 Fabrication of viable tissue-engineered constructs with 3D cell-assembly technique *Biomaterials* **26** 5864–71
- [9] Ouyang L, Yao R, Mao S, Chen X, Na J and Sun W 2015 Three-dimensional bioprinting of embryonic stem cells directs highly uniform embryoid body formation *Biofabrication* **7** 044101
- [10] Zhao Y *et al* 2014 Three-dimensional printing of HeLa cells for cervical tumor model *in vitro* *Biofabrication* **6** 035001
- [11] Lee Y *et al* 2010 Bio-printing of collagen and VEGF-releasing fibrin gel scaffolds for neural stem cell culture *Exp. Neurol.* **223** 645–52
- [12] Yi H *et al* 2005 Biofabrication with chitosan *Biomacromolecules* **6** 2881–94
- [13] Ouyang L, Highley C, Rodell C, Sun W and Burdick J 2016 3D printing of shear-thinning hyaluronic acid hydrogels with secondary cross-linking *ACS Biomater. Sci. Eng.* **2** 1743–51
- [14] Tabriz A, Hermida M, Leslie N and Shu W 2015 Three-dimensional bioprinting of complex cell laden alginate hydrogel structures *Biofabrication* **7** 045012
- [15] Hong S *et al* 2015 3D Printing: 3D printing of highly stretchable and tough hydrogels into complex, cellularized structures *Adv. Mater.* **27** 4034
- [16] Fu Y, Xu K, Zheng X, Giacomini A, Mix A and Kao W 2012 3D cell entrapment in crosslinked thiolated gelatin-poly(ethylene glycol) diacrylate hydrogels *Biomaterials* **33** 48–58
- [17] Khoo Z *et al* 2015 3D printing of smart materials: a review on recent progresses in 4D printing *Virtual Phys. Prototyping* **10** 103–22
- [18] Masaeli E *et al* 2013 Fabrication, characterization and cellular compatibility of poly(hydroxy alcanoate) composite nanofibrous scaffolds for nerve tissue engineering *PLoS One* **8** e57157
- [19] Saracino G, Cigognini D, Silva D, Caprini A and Gelain F 2013 Nanomaterials design and tests for neural tissue engineering *Chem. Soc. Rev.* **42** 225–62
- [20] Cui H, Webber M and Stupp S 2010 Self-assembly of peptide amphiphiles: from molecules to nanostructures to biomaterials *Biopolymers* **94** 1–18
- [21] Hartgerink J 2001 Self-assembly and mineralization of peptide-amphiphile nanofibers *Science* **294** 1684–8
- [22] Hendricks M P, Sato K, Palmer L C and Stupp S I 2017 Supramolecular assembly of peptide amphiphiles *Acc. Chem. Res.* **50** 2440–8
- [23] Webber M *et al* 2011 Supramolecular nanostructures that mimic VEGF as a strategy for ischemic tissue repair *Proc. Natl Acad. Sci.* **108** 13438–43
- [24] Silva G 2004 Selective differentiation of neural progenitor cells by high-epitope density nanofibers *Science* **303** 1352–5
- [25] Tysseling-Mattiace V M, Sahni V, Niece K L, Birch D, Czeisler C, Fehlings M G, Stupp S I and Kessler J A 2008 *J. Neurosci.* **28** 3814–23
- [26] Lee S S *et al* 2014 Gel scaffolds of BMP-2-binding peptide amphiphile nanofibers for spinal arthrodesis *Adv. Healthc. Mater.* **4** 131–41
- [27] Tanimizu N, Miyajima A and Mostov K 2007 Liver progenitor cells develop cholangiocyte-type epithelial polarity in three-dimensional culture *Mol. Biol. Cell* **18** 1472–9

- [28] Jakus A *et al* 2017 'Tissue papers' from organ-specific decellularized extracellular matrices *Adv. Funct. Mater.* **27** 1700992
- [29] Shah R, Shah N, Del Rosario Lim M, Hsieh C, Nuber G and Stupp S 2010 Supramolecular design of self-assembling nanofibers for cartilage regeneration *Proc. Natl. Acad. Sci.* **107** 3293–8
- [30] Zhang S *et al* 2010 A self-assembly pathway to aligned monodomain gels *Nat. Mater.* **9** 594–601
- [31] Auth M *et al* 2005 Preservation of the synthetic and metabolic capacity of isolated human hepatocytes by coculture with human biliary epithelial cells *Liver Transplantation* **11** 410–9
- [32] Auth M 2001 Morphogenesis of primary human biliary epithelial cells: induction in high-density culture or by coculture with autologous human hepatocytes *Hepatology* **33** 519–29
- [33] Patel R *et al* 2014 Microscale bioadhesive hydrogel arrays for cell engineering applications *Cell. Mol. Bioeng.* **7** 394–408
- [34] Ogawa M 2015 Directed differentiation of cholangiocytes from human pluripotent stem cells *Nat. Biotechnol.* **33** 853
- [35] Van Hul N K, Abarca-Quinones J, Sempoux C, Horsmans Y and Le-Clercq I A 2009 Relation between liver progenitor cell expansion and extracellular matrix deposition in a CDE-induced murine model of chronic liver injury *Hepatology* **49** 1625–35
- [36] Lorenzini S *et al* 2010 Characterisation of a stereo-typical cellular and extracellular adult liver progenitor cell niche in rodents and diseased human liver *Gut* **59** 645–54
- [37] Kuramitsu K *et al* 2013 Failure of fibrotic liver regeneration in mice is linked to a severe fibrogenic response driven by hepatic progenitor cell activation *Am. J. Pathol.* **183** 182–94
- [38] Estrach S *et al* 2011 Laminin-binding integrins induce Dll4 expression and notch signaling in endothelial cells *Circ. Res.* **109** 172–82
- [39] Kodama Y, Hijikata M, Kageyama R, Shimotohno K and Chiba T 2004 The role of notch signaling in the development of intrahepatic bile ducts *Gastroenterology* **127** 1775–86
- [40] Geisler F *et al* 2008 Liver-specific inactivation of Notch2, but not Notch1, compromises intrahepatic bile duct development in mice *Hepatology* **48** 607–16
- [41] Li L *et al* 1997 Alagille syndrome is caused by mutations in human Jagged1, which encodes a ligand for Notch1 *Nat. Genet.* **16** 243–51
- [42] McDaniel R *et al* 2006 NOTCH2 mutations cause Alagille syndrome, a heterogeneous disorder of the notch signaling pathway *Am. J. Hum. Genet.* **79** 169–73
- [43] Kamath B M *et al* 2012 NOTCH2 mutations in Alagille syndrome *J. Med. Genet.* **49** 138–44
- [44] Yamada M *et al* 2002 Ile-Lys-Val-Ala-Val (IKVAV)-containing laminin α 1 chain peptides form amyloid-like fibrils *FEBS Lett.* **530** 48–52